

MODELING AND CHARACTERIZATION OF THE EFFECTS OF PERCOLATION FLOW IN COMPOSITES WITH AN EMBEDDED FIBER TOW GAP

Von Clyde Jamora

Director: Oleksandr Kravchenko

Old Dominion University

Fiber reinforced composites are lightweight materials with potential uses in the aeronautics industry. However, novel manufacturing methods cause layup induced defects that propagate through its production. A finite modelling framework is needed to properly simulate the complex non-linear deformations. A heat transfer and a hyperelastic constitutive model was used to simulate the heat transfer and compaction respectively. Experiments were conducted to measure the mass lost during compaction, and the evolution of the fiber volume fraction. Micrographs were taken of the composite for experimental measurements. The angle was measured and were compared between the experimental, a theoretical value and finite element model. Results shows that there is much more physics to be modeled for the compaction of a model with an embedded fiber tow gap. Percolation flow was also found to influence the final morphology from the measurements of the volume of the resin flowing into the gap compared to the reduction in volume of the finite element model and the determined volume of the micrograph from the experiments. This proves that for future finite element analysis work the presence of resin in the fiber tow gap needs to be considered for a proper simulation.

INTRODUCITON

NASA needs lightweight materials, which is outlined in their materials roadmap [1], where the goals are to decrease the mass and reduce the complexity of parts. Composites materials exhibit exceptional strength to weight ratios and can be used to build components for satellites, deployable booms, launch vehicles, and pressure vessels to name a few [4]–[6]. Manufacturing processes such as Automated Fiber Placement (AFP), with its working principle shown in fig. 1(a), allow for fiber-reinforced composites to fulfill these objectives. The composite industry has continued to grow and has become increasingly important for aerospace and aeronautics and with further research, it can accomplish much of NASA's structural requirements.

Novel manufacturing processes allow for complex morphology and precise control over composite layups. These state-of-the-art manufacturing methods allow for high throughput fabrication which would reduce the cost of fabricating parts with complex shapes

[1]. However, these techniques typically result in an irregular morphology which causes defects. These flaws can be traced to initial deposition geometry (fig 1(b)) in combination with the early curing and compaction of the fiber-reinforced composite that takes place before resin gelation. The formation of morphological micro- and meso- structural defect features significantly influences the mechanical properties of composites [2], [3] such as the example shown in fig. 1(c). This shows that for a proper certification of novel manufacturing processes a physics-based finite element process model, the non-uniform morphology must be considered to predict the final morphology formed by the curing and consolidation process.

Furthermore, during compaction, there are two flow modes present for the resin, percolation flow and squeeze flow. Where the percolation flow involves the flow of resin from the fiber bed while the squeeze flow is the flow alongside the fibers. Both these flow modes have a significant potential to affect the

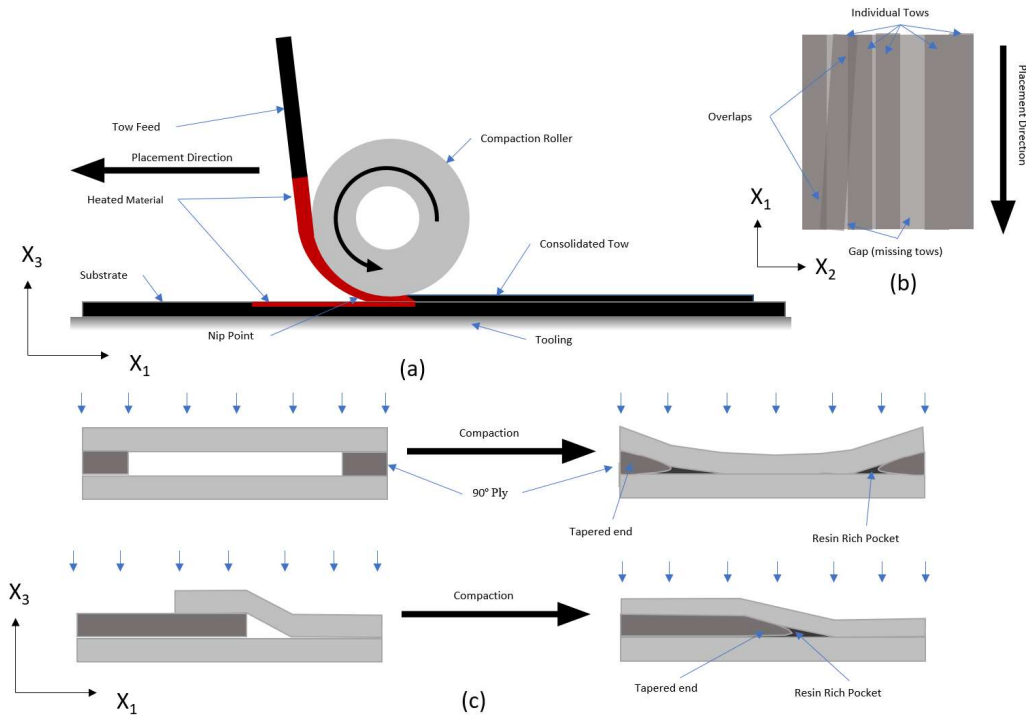


Figure 1. (a) The working principle of an AFP process; (b) Schematic of gaps and overlaps within a ply; (c) Consolidation process at gap and overlap locations.

final morphology of the resin. However, there is not much work exploring the effects of the percolation flow through experimentally and finite element analysis. Therefore, it is important to quantify the effects of the percolation flow on the compaction due to the resin flowing from the fiber bed. This resin bleed out consequently fills layup induced defects such as fiber tow gaps [7], [8]. This manufacturing phenomenon then further affects the resultant fiber angles and consequently changes the mechanical

properties of the composite structure [3], [9]. For a proper simulation-based for predicting the defect morphology, percolation flow needs to be considered. A goal of the project is then to develop an experimentally informed approach to establish the relationship between the resin flow during consolidation and the resultant morphology using finite element analysis (FEA). New composite technologies, such as AFP, can further expand the design space for aerospace applications but needs to a

proper method to understand and predict the layup induced phenomenon [10]–[12].

METHODOLOGY

Experimental Characterization of Defects

Hexcel IM7/8552 with low tack behavior was the composite of choice used in the experiments for the project. The processing conditions of the experimentally made composites were derived from the manufacturer's recommended parameters. Specimens were manufactured using an autoclave. The focus of the experiment was the first 90 minutes of the manufacturer's cycle, which involves the ramp to 110° C with a hold time of 60 minutes. Data was extracted by interrupting the process and measuring the composite. A full vacuum and a pressure of 80 psi were applied to the composite.

Tow gap embedded composite samples were manufactured using the same manufacturing parameters. The stacking sequence of the tow gaps was [0/90/0] with the

gap present at the 90-degree ply as depicted in the symmetrical half shown in fig 2. The length

the full cycle as shown in fig. 3. The mass lost per unit length, weight fraction and the final

fiber volume fraction was then calculated from the six unidirectional samples. Using the images taken during the hold stage interruption the area of the resin lost around the composite sample was measured which was used to calculate the evolution of the fiber volume fraction over time.

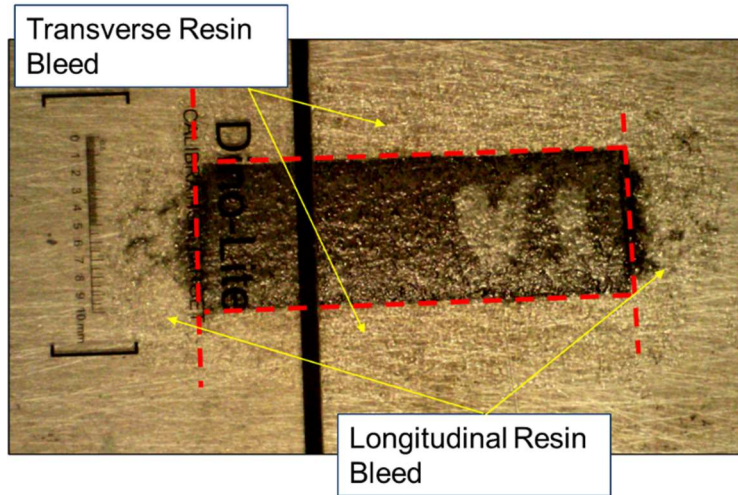


Figure 3. Measurement for the resin bleeds out from the transverse and the longitudinal direction of the composite.

of the sample in the x-direction is 25.4 mm (1 in.) while the gap width is varied between 12.7 mm (0.5 in), 6.35 mm (0.25 in), and 3.175 mm (0.125 in).

Mass loss measurement for unidirectional samples

Unidirectional samples manufactured and were used to calculate a theoretical mass loss due to percolation flow. During the hold stage of the composite cure cycle, the autoclave was interrupted at 5, 15, 30, and 60 minutes to measure the composite mid-cure. The total resin mass weight was then measured of the mass leaking out from the transverse and longitudinal directions of the composite after

After the measurement of the mass, the composite with embedded tow gaps were fully cured in a convection oven at 180° C and observed the resulting morphology at the end of the first hold stage. The tow gap specimens were then cut across the cross section, mounted in resin, and polished. Computer tomography was used to observe the composite's X-Z plane to determine the effects of the curing and compaction on the morphology of the embedded gap, specifically the fiber angle of the top 0° ply. The length of the resin rich region was also measured to compare with the numerical modeling.

Thermo-Chemical Model

Microstructural Characterization of Tow Gaps

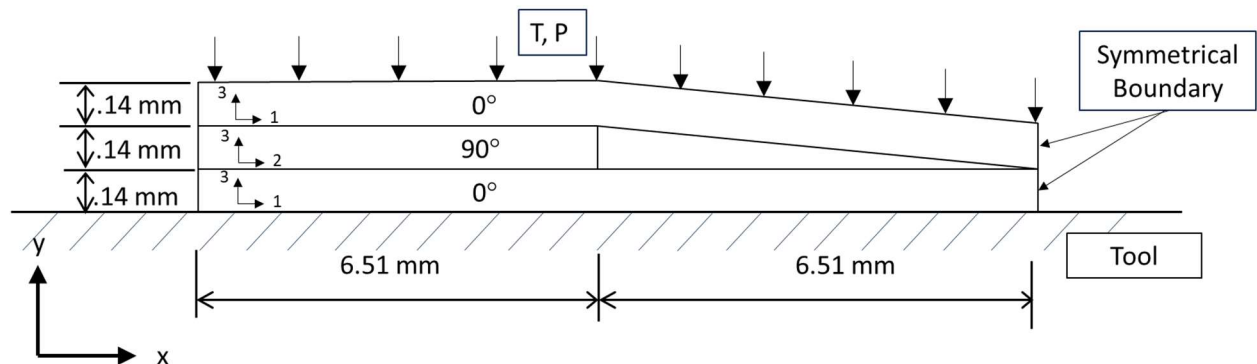


Figure 2. The schematic of the fiber tow gap composite shows the embedded gap between two 0° plies.

Fully understanding the manufacturing phenomenon of the composite requires an interconnected physics model. The model involves a thermo-chemical model which calculates the temperature dependent properties such as a degree of cure and viscosity. The resin chemo-rheology governs the squeezing behavior of the model during the compaction process [13]. The heat transfer is governed by a three-dimensional Fourier heat conduction equation:

$$\rho_c c_c \frac{\delta T}{\delta t} = \nabla \cdot (k \nabla T) + \rho_m v_m Q_t \frac{d\alpha}{dt} \quad (1)$$

where the subscript c and m indicate the homogenized composite and the matrix respectively. The ρ , k , Q_t , v_m , and C indicate the density, thermal conductivity, heat of reaction, fiber volume fraction, and the specific heat, respectively. For the degree of cure, an equation by Hubert was used which is modified from an autocatalytic resin kinetic equation:

$$\frac{d\alpha}{dt} = \frac{K \alpha^{m_\alpha} (1 - \alpha)^{n_\alpha}}{1 + e^{C_\alpha \{\alpha - (\alpha_{c0} + \alpha_{cT} T)\}}} K = A e^{-\frac{\Delta E}{RT}} \quad (2)$$

ΔE is the activation energy, A is a pre-exponential cure rate coefficient, m_α is the first exponential coefficient, n_α is a second exponential coefficient, C_α is a diffusion constant, α_{c0} is the critical degree of cure at $T = 0$ K and finally α_{cT} is a constant that governs the increase in critical resin degree of cure with temperature. The values of the constants can be found in [14]. Using the temperature, and degree of cure from the heat transfer equation, the development of the resin viscosity can be described as:

$$\mu = \mu_\infty e^{k_i \alpha} e^{\frac{U}{RT}} \quad (3)$$

where μ_∞ is a viscosity constant, and U is the activation energy of the viscosity, K_1 and K_2 are temperature independent constants

determined through experimental data. Values of the constants are derived from literature for 8552 resin [15].

Hyperelastic Model

A visco-hyperelastic constitutive equation is used to model the compaction of the uncured composites through FEA. The compaction consists of two components, an elastic and viscous model [16]. The elastic model is derived from hyperelastic transversely isotropic equations which establish the stress equation [17]:

$$\begin{aligned} \sigma &= \sigma^e + \sigma^v = 2 \left(\frac{\partial \psi^e}{\partial \hat{C}} + \frac{\partial \psi^v}{\partial \dot{\hat{C}}} \right) \\ &= \frac{2}{J} \left(\hat{F} \cdot \frac{\partial \psi^e}{\partial \hat{C}} \cdot \hat{F}^T \right) + \sigma^v \end{aligned} \quad (4)$$

The elastic part uses the deformation gradient to calculate the Cauchy-green deformation tensor, \hat{C} , to derive a constitutive equation based on the Helmholtz free energy function and solved using the five invariants of the Cauchy-Green stress tensor. Furthermore, the fiber orientation is updated for each step using the deformation gradient at each node [18]:

$$\hat{P} = \frac{\hat{F} * \hat{P}_0}{\|\hat{F} * \hat{P}_0\|} \quad (7)$$

Where \hat{P} is the fiber direction vector, \hat{F} is the deformation Gradient and \hat{P}_0 is the initial fiber direction vector. The fiber direction is then used in the hyperelastic model, and heat transfer model.

Viscous Model

The approach viscous term is a multiplicative apparent viscosity, which consists of three terms, a strain rate dependent term, and two strain dependent terms [19], [20] as shown in equation 8.

$$\begin{aligned} \hat{\sigma}_{ij}^v &= \hat{\eta}_{rateij} \cdot \eta_{plykk} \cdot \eta_{microkk} \varepsilon_{ij}, kk \\ &= 2,3 \end{aligned} \quad (8)$$

Where $\hat{\eta}_{rate}$ is a strain rate dependent term and η_{ply} and η_{micro} are the strain dependent terms. A novel tensorial viscosity approach was used for the rate term to model the resin flow through a transversely isotropic material. The term assumes the resin behaves as a power-law fluid during compaction which uses the experimentally derived equation for the fiber volume fraction.

$$\eta_{rate_{11}} = 2^{-mf} \left[\frac{\sqrt{\bar{f}}}{1-\sqrt{\bar{f}}} \right]^m \left(\frac{L}{D} \right)^{m+1} \dot{\epsilon}_{11}^{m-1} \quad (9)$$

$$\eta_{rate_{22}} = \eta_{rate_{33}} = 2^{m+1} \left[1 - \sqrt{\bar{f}} \right]^{-m} \dot{\epsilon}_{22}^{m-1} \quad (10)$$

$$\eta_{rate_{23}} = \left[1 - \sqrt{\bar{f}} \right]^{-m} \dot{\gamma}_{23}^{m-1} \quad (12)$$

$$\eta_{rate_{12}} = \eta_{rate_{13}} = 2^{-m} \left[\frac{1 - \sqrt{\bar{f}}}{1 - \sqrt{\bar{f}}} \right]^m \dot{\gamma}_{12}^{m-1} \quad (13)$$

Where the \bar{f} is the ratio of the fiber volume fraction and the maximum packing fraction based on the geometry. L and D are the fiber length and the fiber diameter respectively but for the FEA model, L is the length of the ply in the fiber direction. The power-law exponent m has a value of 0.5 [21]. The rate term can then be multiplied with the strain rate for the viscous stress tensor.

The ply term depends on an analytical solution rearranged by Belnoue [20] which is derived from the no-slip solution from rogers [22]:

$$\eta_{ply_{ii}} = 2 \left(\frac{w_0}{h_0} \right)^2 e^{-4\epsilon_{ii}}, i = 2,3 \quad (14)$$

Where w_0 is the width of the ply, and h_0 is the height of the ply. Since the term is a function of the geometry of the ply. The micro term

depends on phenomenological parameters that are experimentally determined which was adopted from the research done by Nixon-Pearson et al [23] as shown in equation 15

$$\eta_{micro_{ii}} = 2\sqrt{\chi_l} e^{\epsilon_{ii}} k \left(\left(\frac{k}{\sqrt{\chi_f} e^{\epsilon_{ii}} - k} \right)^2 + 3 \right), i = 2,3 \quad (15)$$

Where k is a stepwise function of the temperature, χ_l is the aspect ratio during locking with a value of 0.60 and χ_f is the final aspect ratio of the fiber volume fraction 0.786.

The strain terms are phenomenological parameters that govern the flow model on a microscopic and macroscopic ply scale [23]. Two flow modes are assumed to take place in a fiber reinforced composite. The squeezing occurs initially when the material is treated is incompressible while the percolation flow is the resin leaking from the fiber bed which results in volumetric loss [24].

Finite Element Analysis

A unified modeling approach was developed to model both the heat transfer and the highly non-linear material behavior and the large deformations in the defect regions of the fiber tows during compaction. The computational approach uses an explicit scheme in the commercially available finite element analysis software, Abaqus Unified FEA (Dassault Systemes, Vélizy-Villacoublay, France) with custom-made subroutines.

To simulate the heat transfer using thermo-chemical model and the visco-hyperelastic compaction model, a VUMATHT and a VUMAT subroutine was developed respectively. The contributions of each subroutine are incrementally calculated for each step while state-dependent variables, such as degree of cure and fiber orientation, are recorded. The material properties of IM7/8552

was used and are derived from literature [14], [15], [20] with a density of 1590 kg/m^3 . The pressure and the heat applied to the model is the same processing conditions in the physical experiments. FEA models were made to simulate the physical experiment numerically with the unified physics model.

Previous unidirectional experiments were conducted and compared with the results from simulations with the same conditions and stacking sequences. It proved the model was capable enough to simulate the strain based on the geometry I.E., the number of plies stacked on top or beside each other. Furthermore, it demonstrated that in the first 30 minutes, with points taken at 5, 15, and 30 minutes, the strain of width and the thickness in the compaction model shows non-linear behavior for the compaction of the composite which is typical of a visco-hyperelastic curve. However, at 60 minutes (90 minutes total) into the hold stage, the trend deviates, which indicates some phenomenon may influence the later stages of compaction [9]. This emphasizes the importance of studying the unexplored mechanisms such as effects of the percolation flow's composite and accounting for the resin mass loss in more complex simulation.

RESULTS

Fiber tow gap

The area of interest for the micrograph is at the edge of the 90° where complex non-linear morphology occurs due to the fiber tow gap (fig. 4). In the image, the top 0° ply sinks into the gap and forms a void in the middle of the composite structure. Furthermore, the void is shown to be filled with resin because of the percolation flow from both the 90° and 0° . It can also be noted that the 0° ply shows squeezes into the tow gap which fills a significant portion of the void. To compare and quantify the modeling, the angle was measured between the experiments and the numerical simulation.

The finite element model at 90 minutes is shown in fig. 5. With the measurement of the angles shown in figure 6. As a reference point, the bottom ply was used as a baseline for 0° . The angle measured at the reference point depicted in figure 4 at the micrograph shows an angle of 5.593° and in comparison, the numerical gap model depicts the top ply angle to be 18.480° at 90 minutes at the respective area. The maximum fiber orientation angle measured for the micrograph is 8.63° compared to the 30.20° measured in the numerical model. The distance it took for the angle to reorient towards the x-axis was 1.066 mm for the micrograph compared to 0.39 mm in the numerical model. The gradual slope and the longer distance of the experimental top 0° ply

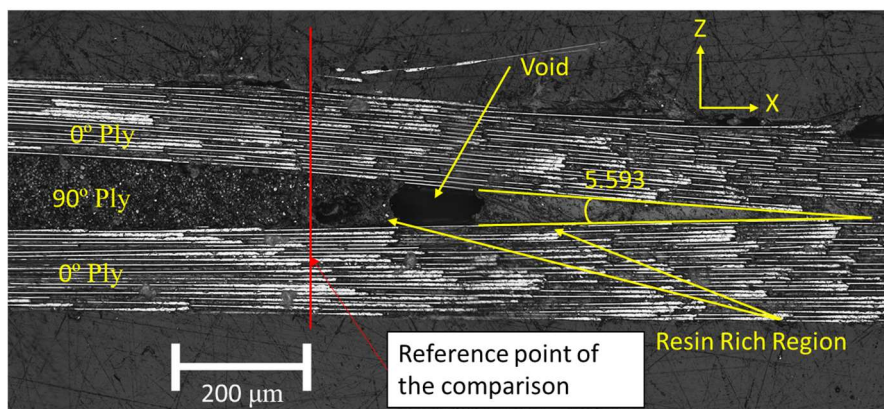


Figure 4. The micrograph of the area of interest at the edges of the 0° ply where the gap begins.

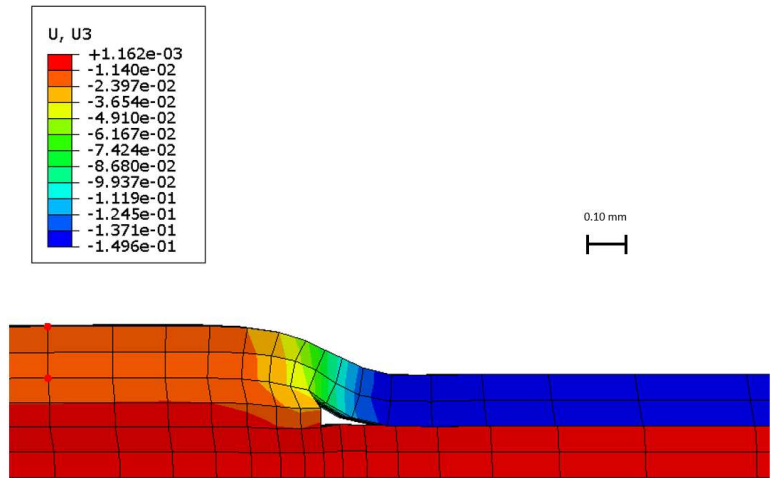


Figure 5. The results of the finite element model after 90 minutes of the simulation time. (60 minutes into the first hold stage of the cure cycle)

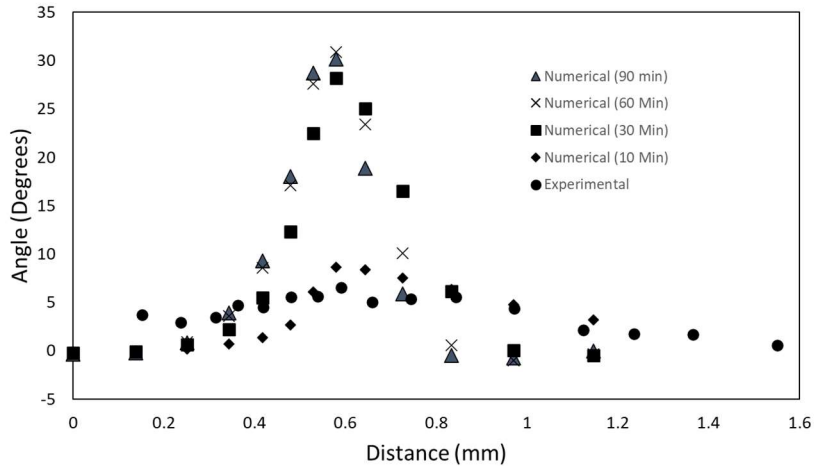


Figure 6. Comparison of the angle of the top ply at various times. Where it shows that at 10 minutes the angle is the closest to the experimentally measured angle.

indicates that improvements need to be made for the model. This shows that some mechanism is preventing the top ply from sinking too fast and maintains a less drastic angle than the 90°. One explanation can be attributed to the percolation flow providing some structural support to the sinking 0° ply. Therefore, the resin flow to the fiber tow gap needs to be characterized.

Mass loss experiment

Using the images taken at cure cycle interruptions, the area of leaking resin, and the deformation measurements were measured.

From the data, the fiber volume fraction can be related linearly to the measured area of the leaking resin. The fiber volume fraction can be then fitted as function of strain in the z-direction or the compaction direction. This would relate the squeeze of the resin with the mass lost through percolation flow. The function was solved as:

$$V_f(\epsilon_{33}) = x(1) * \tanh\left(\frac{\epsilon_{33} + x(2)}{x(3)^2}\right) \quad (16)$$

Where $x(n)$, $n=1,2,3$ fitted parameters, and ϵ_{33} is the strain in the compaction direction. Based

on the area analysis, it is shown that most resin seeps out at the early stages of the cure and compaction. This means that it is necessary to model the percolation flow and the accumulation of the incompressible resin in the fiber tow gap in the finite element analysis at the start of the simulation.

From the weight of the resin that leaked compared to the total weight, the resin weight fraction can be calculated. Expectedly, the mass lost was greater through the transverse direction than the longitudinal direction. However, accounting with the surface area, the longitudinal direction leaks more resin per unit length, with a loss of 2.87 mg/mm, compared to the transverse direction, with a mass loss of 1.98 mg/mm. Using these mass loss values; the amount of resin bleed out can be calculated using the numerical model geometry over time. Based on the orientation of the 0° and 90° plies only the transverse resin flow needs to be considered. The uncured resin through to the fiber tow gap from the side of 90°, the bottom of the top 0° ply, and the top of the bottom 0° ply. The development volume of the fiber tow gap from the model can then be compared with a theoretical volume of the resin from the experiment. A volume of 1.1 kg/m³ and a density of the 8552 was used in for the calculations. Finally, an experimental volume

was measured using the micrograph of the by measuring the area and subsequent volume of the post cure fiber tow gap morphology. Finally, the numerical model volume, theoretical mass loss volume and the experimentally measured volume can be plotted over time to determine at which point does the resin fill the fiber tow gap. The comparison is shown in figure 7. Results show that the resin volume of the model rapidly drops rapidly from 5 to 10 minutes. While the theoretical resin from the leak gradually increases with a common point with the model at 25 minutes. However, when measuring the micrograph, the volume is consistent with the volume found at 12 minutes of the model. This shows that some influence of the resin could be found that keeps the volume of the fiber tow gap consistent. This indicates that some mechanism is needed to simulate the incompressible resin that fills the fiber tow gap, and it can be activated at certain times during the numerical simulation.

Future work

Much of the results show that the percolation flow is large factor in determining the final morphology of the composite structure. This means that some method to incorporate the resin that flows from the composite needs to be simulated in the finite

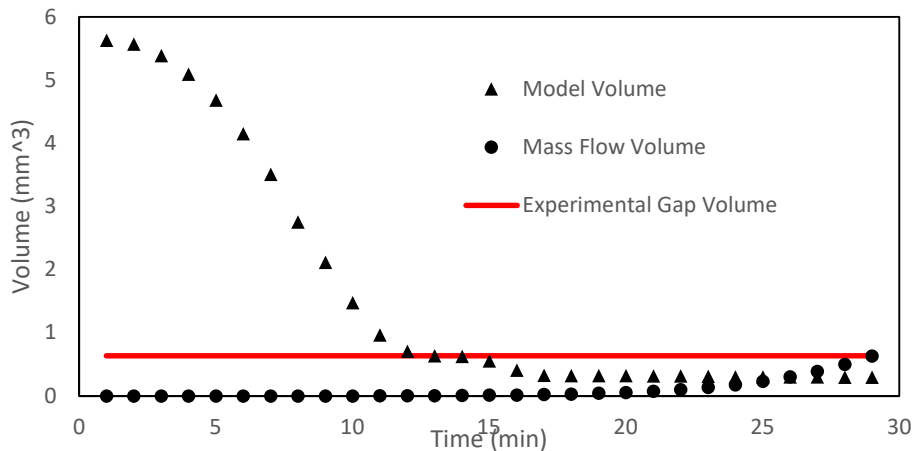


Figure 7. The plot of the experimentally measured volume of the micrograph, the theoretical volume measurement through weight measurement and the finite element model volume.

element model. This includes adding pressure in the insides of the fiber tow gap or incorporating the resin as an incompressible block. Furthermore, incorporating the change in fiber volume fraction could make a more accurate prediction in the compaction. When these components are established, more complex models are planned to be simulated such as more complex layups.

CONCLUSION

A finite element model was developed to simulate the process of manufacturing a carbon fiber composite. Two components were developed for the model, a thermo-chemical to simulate the heat transfer and temperature and hyperelastic components which simulates the compaction. Furthermore, experiments were done to measure the mass flow from the

composites using an autoclave. This involved polishing the sample and observing using microscopy. From the experiment, the mass was measured along with the evolution of the fiber volume fraction of the composite through the images of the leaking resin. A function was derived that fitted the fiber volume with respect to the strain. To compare the results, the angle for the top ply was used as a metric, where it shows that some work is needed to fully simulate the manufacturing of composite. The percolation flow was measured and proved to be a large determining composite morphology. The volume measurements indicate that some mechanism is needed in the finite element model to simulate the physical presence of an incompressible resin that fills the gap due to the percolation flow.

REFERENCES

- [1] K. C. Wu, "Design and analysis of tow-steered composite shells using fiber placement," 2008.
- [2] K. Croft, L. Lessard, D. Pasini, M. Hojjati, J. Chen, and A. Yousefpour, "Experimental study of the effect of automated fiber placement induced defects on performance of composite laminates," *Composites Part A: Applied Science and Manufacturing*, vol. 42, no. 5, Art. no. 5, May 2011, doi: 10.1016/j.compositesa.2011.01.007.
- [3] A. Trochez, V. C. Jamora, R. Larson, K. C. Wu, D. Ghosh, and O. G. Kravchenko, "Effects of automated fiber placement defects on high strain rate compressive response in advanced thermosetting composites," *Journal of Composite Materials*, vol. 55, no. 30, pp. 4549–4562, Dec. 2021, doi: 10.1177/00219983211042073.
- [4] Z. S. Toor, "Space applications of composite materials," *Journal of Space Technology*, vol. 8, no. 1, pp. 65–70, 2018.
- [5] H. M. Y. C. Mallikarachchi and S. Pellegrino, "Design of Ultrathin Composite Self-Deployable Booms," *Journal of Spacecraft and Rockets*, vol. 51, no. 6, pp. 1811–1821, Nov. 2014, doi: 10.2514/1.A32815.
- [6] J.-W. Kim *et al.*, "Assessment of carbon nanotube yarns as reinforcement for composite overwrapped pressure vessels," *Composites Part A: Applied Science and Manufacturing*, vol. 84, pp. 256–265, May 2016, doi: 10.1016/j.compositesa.2016.02.003.
- [7] P. Hubert and A. Poursartip, "A Review of Flow and Compaction Modelling Relevant to Thermoset Matrix Laminate Processing," *Journal of Reinforced Plastics and Composites*, vol. 17, no. 4, pp. 286–318, Mar. 1998, doi: 10.1177/073168449801700402.
- [8] T. G. Rogers and J. O'neill, "Theoretical analysis of forming flows of fibre-reinforced composites," 1991, doi: 10.1016/0956-7143(91)90134-3.
- [9] V. C. C. Jamora, V. M. Rauch, S. Kravchenko, and O. Kravchenko, "Mechanics of Fiber Tow Compaction for Predicting Defect Morphology in AFP composites," in *AIAA SCITECH 2022 Forum*, American Institute of Aeronautics and Astronautics. doi: 10.2514/6.2022-0378.

- [10] K. S. Madhok, *Comparative Characterization of Out-of-Autoclave Materials Made by Automated Fiber Placement and Hand-Lay-Up Processes*. Concordia University, 2013. [Online]. Available: <https://books.google.com/books?id=OovstwEACAAJ>
- [11] D. H.-J. A. Lukaszewicz, C. Ward, and K. D. Potter, "The engineering aspects of automated prepreg layup: History, present and future," *Composites Part B: Engineering*, vol. 43, no. 3, pp. 997–1009, Apr. 2012, doi: 10.1016/j.compositesb.2011.12.003.
- [12] Z. August, G. Ostrander, J. Michasiow, and D. Hauber, "Recent Developments In Automated Fiber Placement Of Thermoplastic Composites," p. 13.
- [13] T. J. Chapman, J. W. Gillespie, R. B. Pipes, J.-A. E. Manson, and J. C. Seferis, "Prediction of Process-Induced Residual Stresses in Thermoplastic Composites," *Journal of Composite Materials*, vol. 24, no. 6, Art. no. 6, Jun. 1990, doi: 10.1177/002199839002400603.
- [14] P. Hubert, A. Johnston, A. Poursartip, and K. Nelson, "Cure kinetics and viscosity models for Hexcel 8552 epoxy resin," *Int SAMPE Symp Exhibit*, vol. 46, pp. 2341–2354, Jan. 2001.
- [15] S. J. Ng, R. Boswell, S. J. Claus, F. Arnold, and A. Vizzini, "Degree of Cure, Heat of Reaction, and Viscosity of 8552 and 977-3 HM Epoxy Resin," NAVAL AIR WARFARE CENTER AIRCRAFT DIV PATUXENT RIVER MD, Mar. 2000. Accessed: Apr. 01, 2021. [Online]. Available: <https://apps.dtic.mil/sti/citations/ADA377439>
- [16] G. Limbert and J. Middleton, "A transversely isotropic viscohyperelastic material: Application to the modeling of biological soft connective tissues," *International Journal of Solids and Structures*, vol. 41, no. 15, Art. no. 15, Jul. 2004, doi: 10.1016/j.ijsolstr.2004.02.057.
- [17] J. Bonet and A. J. Burton, "A simple orthotropic, transversely isotropic hyperelastic constitutive equation for large strain computations," *Computer Methods in Applied Mechanics and Engineering*, vol. 162, no. 1, Art. no. 1, Aug. 1998, doi: 10.1016/S0045-7825(97)00339-3.
- [18] A. J. Favaloro, D. E. Sommer, B. R. Denos, and R. B. Pipes, "Simulation of prepreg platelet compression molding: Method and orientation validation," *Journal of Rheology*, vol. 62, no. 6, Art. no. 6, Oct. 2018, doi: 10.1122/1.5044533.
- [19] P. A. Kelly, "A viscoelastic model for the compaction of fibrous materials," *The Journal of The Textile Institute*, vol. 102, no. 8, pp. 689–699, Aug. 2011, doi: 10.1080/00405000.2010.515103.
- [20] J. P.-H. Belnoue, O. J. Nixon-Pearson, D. Ivanov, and S. R. Hallett, "A novel hyper-viscoelastic model for consolidation of toughened prepregs under processing conditions," *Mechanics of Materials*, vol. 97, pp. 118–134, Jun. 2016, doi: 10.1016/j.mechmat.2016.02.019.
- [21] R. B. Pipes, "Anisotropic Viscosities of an Oriented Fiber Composite with a Power-Law Matrix," *Journal of Composite Materials*, vol. 26, no. 10, pp. 1536–1552, Oct. 1992, doi: 10.1177/002199839202601009.
- [22] T. G. Rogers, "Squeezing flow of fibre-reinforced viscous fluids," *J Eng Math*, vol. 23, no. 1, pp. 81–89, Mar. 1989, doi: 10.1007/BF00058434.
- [23] O. J. Nixon-Pearson, J. P. H. Belnoue, D. S. Ivanov, and S. R. Hallett, "The compaction behaviour of un-cured prepregs: 20th International Conference on Composite Materials, ICCM 2015," Jan. 2015. Accessed: Mar. 29, 2022. [Online]. Available: <http://www.scopus.com/inward/record.url?scp=85044681739&partnerID=8YFLogxK>
- [24] E. L. Wang and T. G. Gutowski, "Laps and gaps in thermoplastic composites processing," *Composites Manufacturing*, vol. 2, no. 2, pp. 69–78, Jan. 1991, doi: 10.1016/0956-7143(91)90182-G.